10th International Conference on Fracture Mechanics of Concrete and Concrete Structures
FraMCoS-X
G. Pijaudier-Cabot, P. Grassl and C. La Borderie (Eds)
https://doi.org/10.21012/FC10.233322

EXPERIMENTAL AND NUMERICAL STUDY OF CRACK PROPAGATION WITH THE PHASE FIELD METHOD: APPLICATION TO THREE-POINT BENDING TEST

A. TSITOVA[†,††,*], F. BERNACHY-BARBE[†], B. BARY[†] AND F. HILD[††]

[†]Den-Service d'Etude du Comportement des Radionucléides (SECR),
CEA, Université Paris-Saclay,
91191 Gif-sur-Yvette, France
*main author: e-mail: aliaksandra.tsitova@cea.fr

[††]LMT UMR 8535 (ENS Paris-Saclay, CNRS, Université Paris Saclay),
61 avenue du Président Wilson, 94235 Cedex Cachan, France

Key words: crack, phase-field, fracture energy, quasi-brittle, mortar.

Abstract: The safety of double wall Concrete Containment Buildings (CCBs) primarily depends on the integrity of concrete. The delayed deformations of concrete induced by creep and shrinkage cause the loss of pre-stress that may reduce the air-tightness of the CCB internal wall in accidental conditions. Creep of concrete is a complex phenomenon and its rate depends on several factors among which microcracking is of major significance. To be able to represent effectively creep/microcracking couplings in concrete with a mesoscale numerical model, a reliable damage model has to be primarily defined. The phase field method for the modeling of fracture in brittle materials implemented in the finite element software Cast3m is chosen as a basis. The interest of the study is to identify consistent phase-field parameters for mortar and cement paste. The study is carried out by comparison of experimental and numerical three-point notched bending tests using experimental elastic properties and boundary conditions measured with Digital Image Correlation (DIC). Parameter identification is performed using DIC measurements on three-point notched beam bending tests and validated in 3D cases.

1 INTRODUCTION

The safety of double wall Concrete Containment Buildings (CCBs) that are widely used in the French nuclear industry primarily depends on the integrity of concrete. The containment building is the final barrier implemented to protect the public from radioactive substances released during an accident inside the containment. Sometimes called the third containment barrier for French reactors, it must provide confinement of radioactive species in the event of failure of fuel rod cladding (first barrier) and reactor coolant system (second barrier).

The double wall CCB undergoes accelerated creep and shrinkage kinetics as compared to a single wall due to its particular environmental conditions (heated air of reactor, absence of rehydration from outside).

The consequence of creep and shrinkage is increased risk of potential leaks under proof-testing or accidental high internal pressure. The structure may develop local tensile stresses due to the relaxation of pre-stresses. The cracks formed at young age or under drying, closed due to pre-stressing, may be re-opened. The local tensile stress state of concrete can be sufficient to initiate new cracks [1].

In view of this issue, the prediction of delayed deformations and subsequent mechanical property degradation is of major interest. To be able to accurately describe creep/microcracking couplings in concrete in a mesoscale analysis, a reliable damage model has to be first defined.

The phase field method for the modeling of fracture in brittle materials [2] implemented in the finite element software Cast3m is chosen as a basis. The interest of the study is to identify consistent phase-field parameters for mortar and cement paste. The study is conducted by comparing experimental data and numerical predictions of three-point notched bending tests using experimental elastic properties and boundary conditions measured with Digital Image Correlation (DIC).

2 MODELING THE FRACTURE WITH THE PHASE FIELD METHOD

Phase field model has been proven to be an effective tool for crack modeling in brittle materials. In this section, a short review of the thermodynamic and energetic approach of Miehe et al. [2],[3] is presented.

Sharp crack topologies are regularized by introducing a diffusive crack zone. The crack surface is described by a functional Γ dependent upon an auxiliary variable d (*crack phase field)* and *characteristic length l*

$$\Gamma_l(d) = \int_\Omega \gamma_l\,(d) d\Omega \tag{1}$$

$$\gamma_l = \frac{d^2}{2l} + \frac{l}{2}|\nabla d|^2 \tag{2}$$

where γ_l is the crack surface density (with $d = 0$ characterizing the unbroken state and $d = 1$ the fully broken state of the material). To bring in continuous principles, the damage variable d is gradually changing from $x = 0$ corresponding to the cracked surface, and $x = l$, where the body is considered intact (Figure 1).

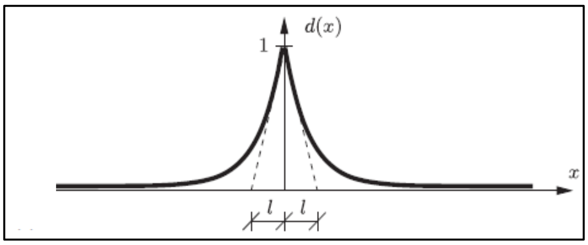

Figure 1 : 1D diffusive crack zone [3]

The minimization problem for the crack surface $d = \arg\left\{\inf_d \Gamma^l\,(d)\right\}$ gives the crack phase field function

$$d(x) = e^{-|x|/l} \tag{3}$$

The total energy is equal to the sum of the bulk energy E_e and the energy required for crack propagation E_d. Based on Griffith's theory

$$E_d = \int_\Omega \psi_d d\Omega = \int_\Omega G_f\,\gamma_l(d)\,d\Omega \tag{4}$$

where G_f is the fracture energy. The degraded bulk energy is derived for the case of tensile induced rupture with a split in positive and negative energy contributions.

$$E_e(d,\varepsilon) = \int_\Omega \psi_e d\Omega \tag{5}$$

$$\psi_e(d,\varepsilon) = (g(d) + k)\psi_0^+(\varepsilon) + \psi_0^-(\varepsilon) \tag{6}$$

where $\psi_0^+(\varepsilon)$ is the "positive" extension energy, $\psi_0^-(\varepsilon)$ the "negative" contraction energy, $g(d) = (1-d)^2$ the *degradation function*. As $g(d)$ is specifically associated with the extension energy, it allows the stiffness recovery to be modeled in contraction due to crack closure.

The variational derivative of the potential energy for irreversible process reads

$$\sigma\!:\dot{\varepsilon} = \dot{\psi} + \phi\ ,\ \phi \geq 0 \tag{7}$$

where σ is the Cauchy stress tensor, $\dot{\varepsilon}$ the strain rate, $\dot{\psi}$ the free Helmholtz power, and ϕ the dissipated power.

The free Helmholtz energy is expressed as

$$\dot{\psi} = \dot{\psi}_e + \dot{\psi}_d = \frac{\partial\dot{\psi}}{\partial d}\cdot\dot{d} + \frac{\partial\dot{\psi}}{\partial\varepsilon}\!:\dot{\varepsilon} \tag{8}$$

The minimization of Eq. (7) gives a

thermodynamically consistent phase field equation for the damage variable *d*

$$\left(\frac{G_f}{l} + 2\mathcal{H}\right) \mathrm{d} - G_f l \Delta \mathrm{d} = 2\mathcal{H} \quad (9)$$

$$\mathcal{H}_n = max\{\psi_{n-1}^{+}, \psi_n^{+}\} \quad (10)$$

The temporal changes of the phase field is driven by a *local history field* $\mathcal{H}$, which is equal to the maximum tensile strain obtained in the history of $\psi_0^{+}(\varepsilon)$.

3 EXPERIMENTAL TESTS

3.1 Introduction

Experimental tests were performed to measure the mechanical properties (Young's modulus, Poisson's ratio, fracture energy, tensile strength) on mortar and cement paste VeRCoRs (VErification Réaliste du Confinement des Réacteurs) [4] for modeling purposes. The formulations for cement and mortar are derived from the VeRCoRs concrete formulation that is used in laboratory tests (Table 1). The water to cement ratio is W/C = 0.525. The mortar formulation represents the matrix surrounding the coarse aggregates, and the cement paste formulation corresponds to the matrix surrounding the fine aggregates in the mortar.

Table 1 : Material constituents

Constituents	Mass (kg)	Density (kg/m^3)
Mortar		
Cement CEM I 52.5 N CE CP2 NF Gaurain	320	3.1
Sand 0/4 REC LGP1 thresholded to 2 mm	680.6	2.6
Sikaplast Techno 80	2.6	1.1
Addition water	169.8	1.0
Total water	171.8	1.0
Cement paste		
Cement CEM I 52.5 N CE CP2 NF Gaurain	320	3.1
Total water	167.9	1.0

The specimens were stored at ~100% relative humidity before the tests that were carried out at 28 day age.

3.2 Compression tests

The Young's modulus, Poisson's ratio and compressive strength were determined by means of compression tests on cylindrical specimens of size Ø30 × 65 mm. Compression tests were performed in a closed-loop displacement-controlled machine with 250 kN capacity. The longitudinal and transverse strains were measured with strain gages glued with X60 HBM® adhesive. The force was measured with the load cell of the testing machine.

3.3 Three-point bending tests

The fracture energy of cement paste and mortar was measured based on the three-point bending tests on notched prisms 4 × 4 × 16 cm in size. Notches 12mm in length were cut with a wire saw. Bending tests were performed with a closed-loop displacement-controlled machine. The stroke velocity is 0.03 mm/min, which allows steady crack propagation to be achieved [5]. The loading block and both supports can rotate about their axes in the direction of the specimen axis. The force is measured by the load cell of the 250-kN testing machine. The CMOD is measured using a clip gage, which is attached to metal plates glued on both sides of the notch with a base length of 9 mm (Figure 2).

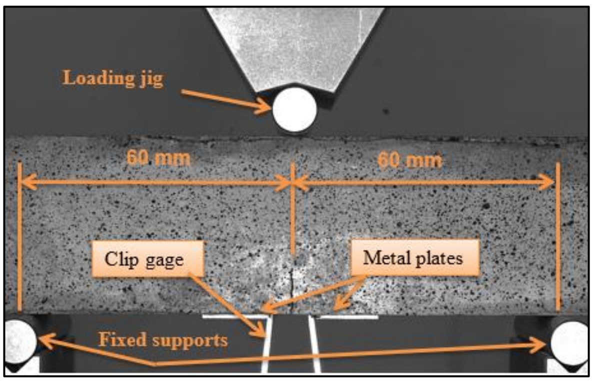

Figure 2 : Experimental setup for three point bending test

The fracture energy is calculated based on the CMOD-force curve [5]

$$G_f = \frac{0.75W_0^c + W_1^c}{A_{lig}} \tag{11}$$

with

$$W_1^c = 0.75\left(\frac{S}{L}m_1 + 2m_2\right) g \cdot CMOD_c \tag{12}$$

where W_1^c is the area below CMOD curve up to the failure of the specimen, W_1^c the work done by the deadweight of the specimen and loading jig, $CMOD_c$ the CMOD at failure, A_{lig} the area of the broken ligament, m_1 the mass of the specimen, S the loading span, L the total length of specimen, m_2 the mass of the jig not attached to the testing machine but put on specimen.

3.4 Digital image correlation

The three-point bending tests were monitored with a camera on one side during the test with 1.5 to 2.0 fps acquisition rate for the following DIC analyses. DIC enables for measuring displacement fields of specimen surfaces during the whole test [6]. To improve DIC performances, a random "speckle" pattern can be sprayed onto the surfaces of interest.

Global DIC is used for measuring displacement fields of specimens during the tests. Also, this technique is an effective tool for detecting and quantifying crack propagation.

3.5 Brazilian tests

The tensile strength was measured by means of Brazilian tests on disks Ø30 × 15 mm. Tests were carried out with a closed-loop displacement control based machine with 20 kN capacity.

4 NUMERICAL EXAMPLES

4.1 Benchmark and parametric study

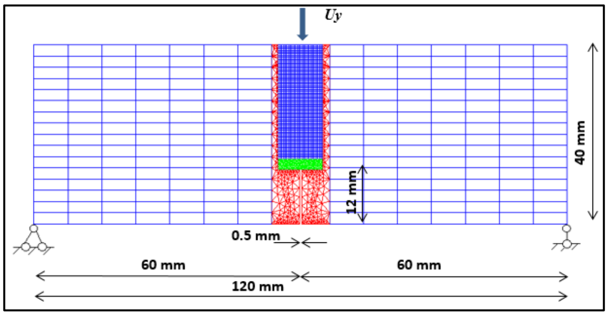

Figure 3 : Mesh geometry for a benchmark three-point bending test

The mesh geometry replicates the specimen geometry (Figure 3). The mesh in the fracture initiation and propagation zone is discretized with quadrangle elements of dimension h_{min} = 0.4 mm. The size of elements is increasing from the expected damage zone toward boundaries. The vertical load is prescribed as the sequence of vertical displacements $U_y(t) = m\Delta U_y$, applied in the middle top point with the integer m ranging from zero to the number of simulated time steps N and with ΔU_y a constant incremental displacement.

Table 2: Input parameters for the phase field model

	Cement paste	Mortar
Young's modulus, GPa	13.3	28.9
Poisson's ratio	0.26	0.2
Fracture energy, N/m	4.5	52.0
Characteristic length l, mm	1.5	1.5
$U_{y,max}$, mm	0.03	0.1

The Young's modulus and Poisson's ratio were determined in compression tests described in Section 3.2 as the average for 3 specimens (see Table 2).

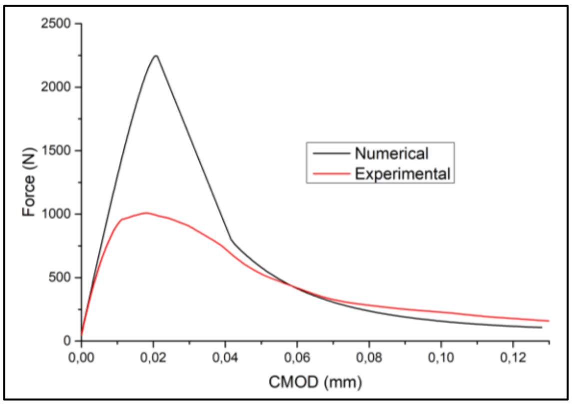

Figure 4 : Experimental and numerical force-CMOD curves for mortar

The comparison of numerical and experimental force-CMOD curves reveals discrepancy of the peaks corresponding to the rupture (Figure 4). Following Equation (4) and Griffith's theory, crack initiation in this model is governed by the fracture energy G_f. In order to compare the energy contribution needed for crack initiation in experiments and numerical simulations, $G_{f,pre-peak}$ is calculated with the integral of force-CMOD curve until F_{max} and compared to the full energy. Experimental and numerical values are given in Table 3. Experimental values are the average of 3 tests for the mortar and 4 tests for the cement paste.

Table 3 : Experimental and numerical fracture energy

	Mortar	Cement paste
	Experiment	
G_f^{exp}	52.7 N/m	6.6 N/m
$G_{f,pre-peak}^{exp}$	7.52 N/m	1.4 N/m
$\frac{G_{f,pre-peak}^{exp}}{G_f^{exp}}$	14.2%	20.7%
	Prediction	
G_f input value	52.0 N/m	4.5 N/m
G_f^{num}	55.6 N/m	4.6 N/m
$G_{f,pre-peak}^{num}$	39.2 N/m	3.6 N/m
$\frac{G_{f,pre-peak}^{num}}{G_f^{num}}$	70.7%	79.7%

The comparison of $\frac{G_{f,pre-peak}}{G_f}$ shows an important misbalance in energy necessary for failure in experiments (14% for mortar and 21% for cement paste) and numerical simulations (71% for mortar and 80% for cement paste). Keeping the same numerical model, the displacement control mode was changed into the experimental force. Such change led to the fact that G_f = 10 N/m gives a good agreement on the peak force for mortar.

Other features that can be observed from Figure 4 is the absence of nonlinear pre-peak behavior and steady post-peak propagation.

Energy discrepancies and mostly linear pre-peak behavior can be the consequence of the small size of the fracture process zone (FPZ) as the value $l = 1.5$ mm was initially chosen to be in agreement with the mesh size. Characteristic lengths can be selected as $l = \frac{EG_f}{f_t^2}$ [7]. Based on the experimental measurements, for mortar l varies within the range 32-52 mm, and for the cement paste as 7-11 mm. To study the effect of characteristic length on the non-linearity of the response, several values were tested. In Figure 5, the force-CMOD curves with varying l are reported. The loading is the experimental force history presented in Figure 4. The fracture energy is set equal to 10 N/m.

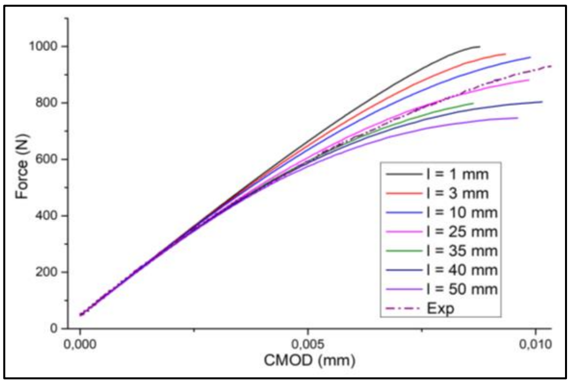

Figure 5: Effect of the characteristic length on the pre-peak response

It is observed that an increase of characteristic length induces more pronounced non-linear pre-peak responses, and decreases the ultimate load. Values between l = 25 mm and l = 35 mm are observed to give a good agreement on the pre-peak part. However, due to the important size of the diffusive crack zone, once the damage variable reaches $d = 1$, the simulation experiences convergence issues.

In Figure 6, $G_f = 10$ N/m and l = 35 mm give a good agreement in the pre-peak part. However, the simulated failure is always brittle, without a steady crack propagation.

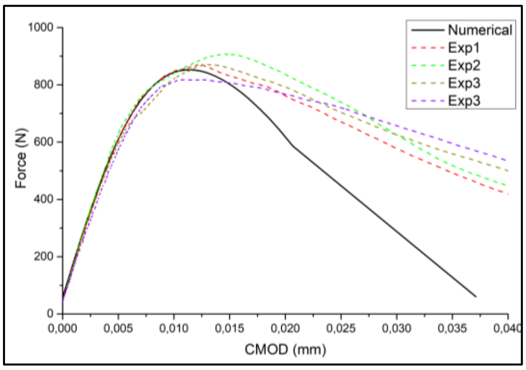

Figure 6: Comparison of numerical and experimental force-CMOD curves (input G_f = 10 N/m, l_{ch} = 35 mm)

For the cement paste, crack propagation is considerably influenced by the details of its microstructure (e.g., porosity, elevated W/C ratio areas) and local defects (e.g., air bubbles, drying microcracks). The variability of experimental results is more important and finding the parameters to fit the experimental data is more challenging. Numerical simulation of the average calculated values $G_{f,pre-peak}^{exp}$ = 1.5 N/m and $l = 10$ mm gives a good agreement with the experimental peak force.

4.2 Crack propagation study

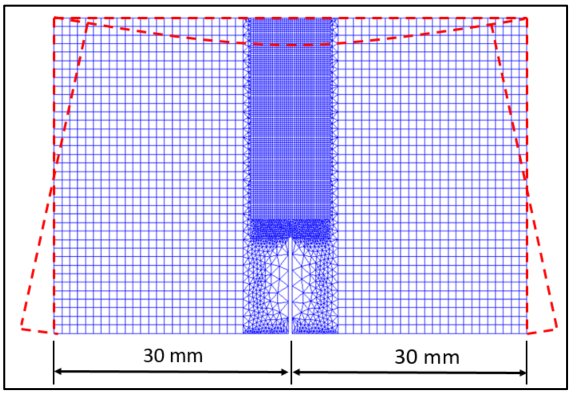

Figure 7: Mesh geometry and precribed displacements

In the second part of the study, the realistic crack path is modeled using as boundary conditions the experimental displacement fields. The geometry is reduced only to the middle part of the beam. The measured displacements are applied at mesh points with 0.3 mm step on top and lateral boundaries as illustrated in Figure 7. They were measured with global DIC. The material properties for mortar were taken as indicated in Table 2.

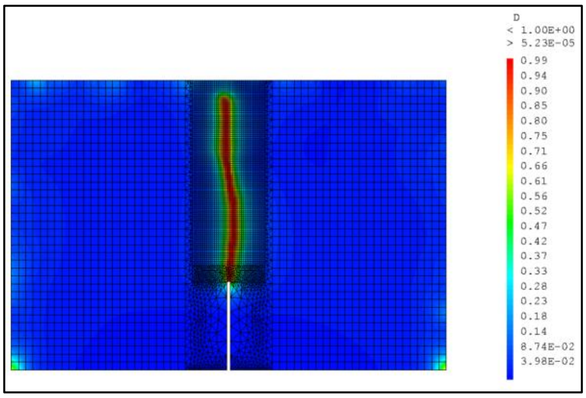

Figure 8 : Numerical crack path computed with DIC displacements

The control of the vertical and horizontal displacements allows to model realistic and complex crack geometry even for the case of homogeneous structure (with no inclusions or other types of heterogeneities, see Figure 8). The comparison of CMOD histories shows a good agreement (Figure 9). However, it was observed that due to explicit displacement field control, the fracture initiation no longer depended on G_f.

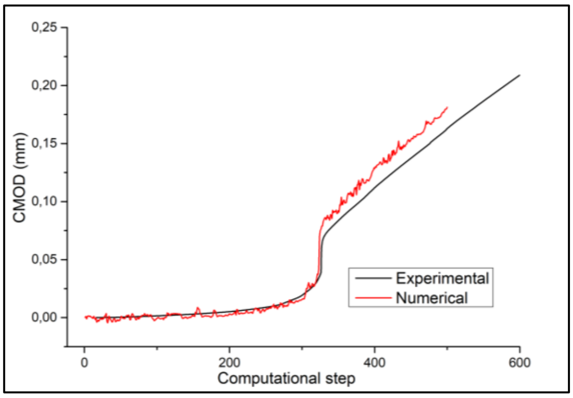

Figure 9: Experimental and numerical CMOD history

5 CONCLUSIONS

In this study, an elastic brittle phase-field model was applied to the case of three-point bending tests for mortar and cement paste. The influence of the characteristic length on the non-linear pre-peak behavior was investigated. The fracture energy G_f was adapted to represent rather a local fracture energy than global. The material parameters (characteristic length, fracture energy) were obtained to give a good agreement in terms of pre-peak response and ultimate load.

However, modelling post-peak steady crack propagation remained challenging. Further developments are needed (e.g., CMOD control of the simulations). Further, 2D simulations propose a rather simplified cracking model. To represent explicitly quasi-brittle failure, 3D and mesoscale models will be developed. The enrichment of the model is also possible by the introduction of viscoelasticity of the cementitious matrix.

REFERENCES

[1] E. Gallitre, P. Labbe, G. Pastor, and Y. Le Pape, 'Durée de vie des enceintes de confinement', *Revue Générale Nucléaire*, pp. 43–47, Mar. 2014.

[2] C. Miehe, M. Hofacker, and F. Welschinger, 'A phase field model for rate-independent crack propagation: Robust algorithmic implementation based on operator splits', *Computer Methods in Applied Mechanics and Engineering*, vol. 199, no. 45, pp. 2765–2778, Nov. 2010.

[3] C. Miehe, F. Welschinger, and M. Hofacker, 'Thermodynamically consistent phase-field models of fracture: Variational principles and multi-field FE implementations', *Int. J. Numer. Meth. Engng.*, vol. 83, no. 10, pp. 1273–1311, Sep. 2010.

[4] S. Huang, 'Comportement vieillissant du béton en fluage : application au béton VeRCoRs', PhD thesis, Université Paris-Est, 2018.

[5] 'Method of test for fracture energy of concrete by use of notched beam, JCI-S-001-2003'. Japan Concrete Institute Standard.

[6] S. Roux, J. Réthoré, and F. Hild, 'Digital Image Correlation and Fracture: An Advanced Technique for Estimating Stress Intensity Factors of 2D and 3D Cracks', *Journal of Physics D: Applied Physics*, vol. 42, p. 214004 (21pp), 2009.

[7] A. Hillerborg, M. Modéer, and P.-E. Petersson, 'Analysis of crack formation and crack growth in concrete by means of fracture mechanics and finite elements', *Cement and Concrete Research*, vol. 6, no. 6, pp. 773–781, Nov. 1976.